Supplementary Information : Autonomous Engulfment of Active Colloids by Giant Lipid Vesicles

Florent Fessler, Martin Wittman, Juliane Simmchen, and Antonio Stocco
(Dated: June 2, 2024)

Appendix A: Effect of the white light illumination on the particle velocity

For a given concentration of glucose, changing the intensity of the white light illumination also modulates the measured projected active velocity V from MSD fits. While the experiments conducted in this work were performed at low white light illumination intensity (40% of maximum intensity), we show in Figure 1 that the average V extracted for $N = 10$ particles increase with increasing illumination intensity, as it was the case for blue light (see main text).

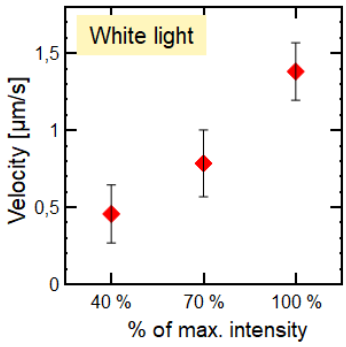

FIG. 1. Average (on N= 10 trajectories) measured values for projected velocity V for different illumination intensities (in percentage of maximum illumination intensity) at 100 mM glucose concentration.

Appendix B: Translational diffusion of free particles in glucose

Using equation Eq.(1) from the main text, we can extract both the projected active velocity and the translational diffusion coefficient D_{tr} of the Janus particles. Values for the extracted projected velocity V are reported in the main text and V increases with increasing glucose concentration. Here, Figure 2 shows the values for D_{tr} as a function of the glucose concentration. We show that for lower glucose concentrations, the values are in agreement with Fàxen predictions of the diffusion coefficient of a particle close to a solid wall at a distance $h = 0.2R_P = 300$ nm [1]. For increasing glucose concentrations, D_{tr} increases and becomes closer to the Stokes-Einstein prediction of the diffusion coefficient valid in the bulk. This suggests that the particle activity may have an impact on the swimming distance of the particle from the substrate or that additional short time noises due to the particle activity are present, which result into higher effective diffusion coefficients.

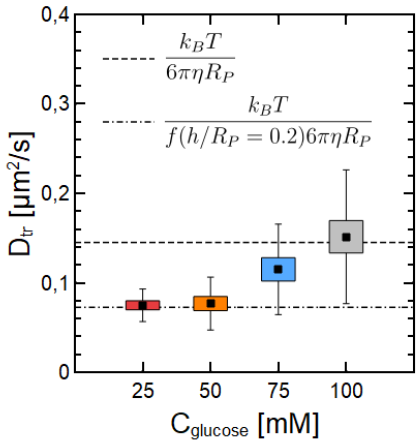

FIG. 2. Average (over N= 10 trajectories for each point) of the values extracted from MSD fits for the projected velocity V for different illumination intensities (in percentage of maximum illumination intensity) at 100 mM glucose concentration. Error bars account for the standard deviation.

Given that the wrapped particle and the membrane neck form a connected object, additional dissipations arising from the membrane viscosity can contribute to the drag. The drag experienced by the neck is in fact equivalent to the drag of a disk embedded in a lipid membrane as modelled by Saffman-Delbrück [2]. Hence, the drag increase can be explained by this model, which also points to a very small gap between the particle and the wrapping membrane.

Appendix C: Membrane tension measurement from large wavelength undulations of floppy vesicles

GUVs used in these work were prepared following the exact same protocol as the one in [3]. Osmotic deflation leads to floppy vesicles showing thermal undulations of the membrane visible under the microscope. Tensions of the order of $\sigma \sim 10^{-8}$ N.m^{-1} were measured by the force of pulling a tube behind a wrapped particle with optical tweezers.

These tension measurements can be verified by analyzing the large wavelengths ($\lambda \gg \sqrt{\kappa/\sigma}$) thermal

undulations of GUVs. In the following, we show that the tension of the vesicles in which autonomous engulfment of active colloids occurred lays in the range $\sim 10^{-8}$ N.m^{-1} by using the approach reported by Turlier *et al.* [4].

Using the Monge representation, the shape of the vesicle can be described using the height vector $(x, y), h(x, y) = (\mathbf{r}, h(\mathbf{r}))$, where we consider only small deformations $|\nabla h(\mathbf{r})| \ll 1$. In Fourier space and by applying the equipartition theorem considering that the system is at equilibrium, the mean squared amplitude of the Fourier component $\langle |h_\mathbf{q}|^2 \rangle$ for the wave-vector $\mathbf{q}$ reads [5]:

$$\langle |h_\mathbf{q}|^2 \rangle = \frac{k_B T}{\sigma \mathbf{q}^2 + \kappa_b \mathbf{q}^4} \tag{C1}$$

We can integrate the static fluctuation spectrum Eq. C1 over wave-vectors in the range $[q_{min}; q_{max}]$ where $q_{min} = 2\pi/L$ and $q_{max} = 2\pi/a$ are cutoffs due to the limited deformations of a real vesicle membrane with $L \approx \sqrt{4\pi R_v^2}$ a typical size associated to the vesicle and $a \approx 1$ nm the scale at which smallest deformations can occur. Making sure that $a \ll L$, one obtains [4]:

$$\langle |h|^2 \rangle = \frac{k_B T}{4\pi\sigma} \ln\left(1 + \frac{\sigma}{\kappa_b q_{min}^2}\right) \tag{C2}$$

In a regime where undulations are determined by tension, $q \ll 2\pi\sqrt{\sigma/\kappa_b}$. Thus, for large wavelength undulations, the modes in q^2 dominate and the mean squared amplitude of the undulations can be estimated by Eq. C2.

In Figure 3A,B and C, we show how we experimentally extract the contour of a vesicle at the equator using fluorescence microscopy and translate it into $h(\theta) = R(\theta) - R_0$. It appears clearly for a representative case that the amplitude of the long wavelengths undulations of h in real space are of the order of $\sqrt{\langle |h|^2 \rangle} \sim 200 - 300$ nm. Through Eq. C2 (Black in Figure 3D) we can confirm that such amplitude corresponds to a range of membrane tensions spanning between $\sigma = 10^{-9}$ and $\sigma = 10^{-7}$ N.m^1, which is consistent with measurements in Ref. [3].

This measurement provides an order of magnitude for the tension, which agrees with the tension measurement obtained by the pulling force of a tube by optical tweezers.

Appendix D: Particle orientation tracking and correlation with motion persistence

Tracking of the orientation was performed using a method implemented previously for fluorescent Platinum

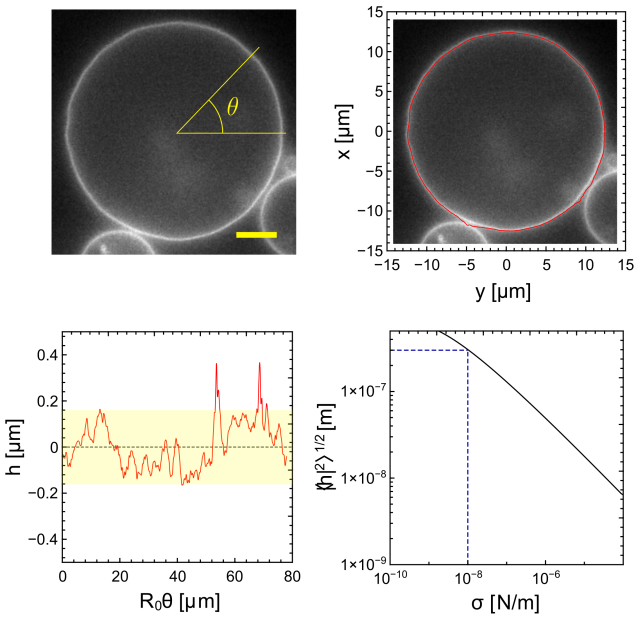

FIG. 3. (a) Fluorescence snapshot of a vesicle after osmotic deflation and engulfment of a Cu@SiO_2 particle. (b) Extraction of the vesicle contour using ImageJ. The scalebar is 5 µm. (c) Variations of $h(\theta) = R(\theta) - R_0$ along the contour, where R_0 is the radius of the ideal circle from which the thermal undulations make the real membrane deviate (d) Plot of $\sqrt{\langle |h|^2 \rangle}$ Eq. C2 allowing to visualize the expected amplitude of large wavelengths undualtions for a given membrane tension. The blue dashed line stands for the tension and fluctuation amplitudes in the representative case of (c).

coated particles. The method is depicted in Figure 4 and will be exposed in the following. Using ImageJ, one can threshold the image in order to have a binary image with only the copper cap visible (which has lower pixel intensity than the background and the bare hemisphere of the Cu-SiO_2 Janus). Fitting an ellipse to the half-moon shaped cap allows to determine the angle between the long axis of the ellipse and a fixed axis on the image. An ImageJ routine allows to repeat this for each frame of a movie, providing an orientation trajectory. The associated tracking error is low provided that the particle out-of-plane orientation does not significantly deviates from $\alpha = \pi/2$, where α is the angle between the substrate normal and the normal of the plane containing the Janus boundaries .

We can check both the robustness of this orientation tracking technique and the activity of Cu-SiO_2 particles in glucose by comparing the evolution of ϕ (the output angle of the tracking, see Figure 4) and θ, which is the angle characterising the active motion persistence obtained from center-of-mass tracking of the particle (done using the tracking method exposed earlier) with a sliding average over 10 points to remove the Brownian translational noise. Figure 5 shows the good agreement between the observed direction of motion and the tracked orientation,

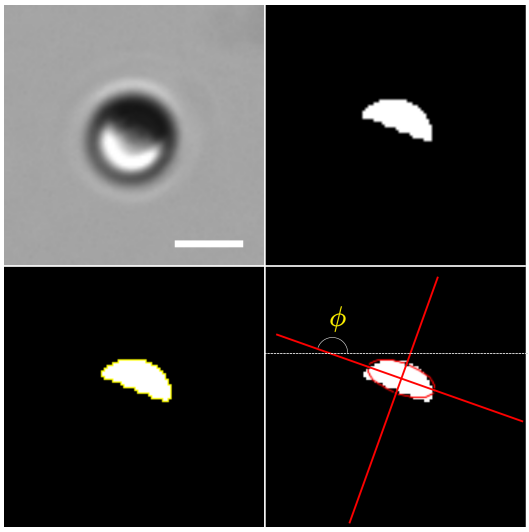

FIG. 4. Procedure of orientation tracking using ImageJ. Top left panel shows the raw bright field image. Top right panel shows the same image but thresholded to obtain a binary image and subsequently inverted to have the dark cap appearing as maximum pixel value. Lower left panel shows the contour obtained using the "Wand" tool of ImageJ. Lower right panel shows the ellipse fitted (in red) to the contour, and the angle that makes the long axis of this ellipse with a fixed axis of the frame which we call ϕ (in-plane orientation).

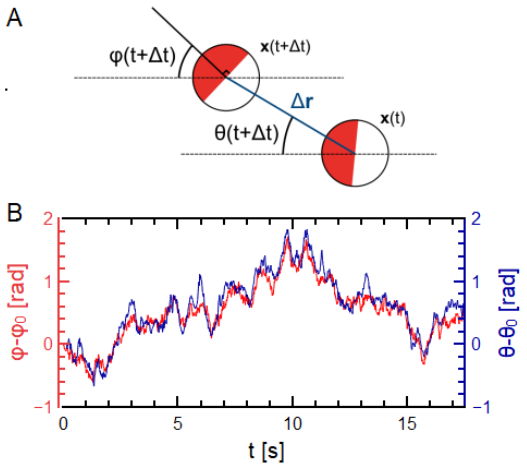

FIG. 5. (a) Sketch defining the orientation ϕ and the direction of motion θ of a Janus swimmer. (b) Temporal evolution of $\phi - \phi_0$ and $\theta - \theta_0$ where $\phi_0 = \theta_0 = 0$. The curve of $\theta - \theta_0$ was obtained by performing a sliding average over $N = 20$ points to get rid of the noise arising from short times brownian motion and evidence the direction given by the active propulsion force.

confirming both the accuracy of the tracking method and the directed active propulsion of the particle in glucose.

Appendix E: Rotational friction in the capture phase

During the capture phase, the angular confinement in the geometry of interest allows to track the orientation of the particle with the routine exposed previously. Figure 6 shows the mean squared angular displacement of a particle during the capture for a trajectory of 62 seconds with an acquisition frequency of 100 Hz yielding good statistics. The log-log scale graph allows to see the diffusive behavior at short times and confined orientational motion at long times with the appearance of a plateau of magnitude $\langle(\phi - \beta)^2\rangle = 0.22$ rad^2. The linear scale inset shows how the measured linear diffusion (with $D_{tr} = 0.056$ s^{-1}) compares to the theoretical rotational diffusion coefficient in the bulk.

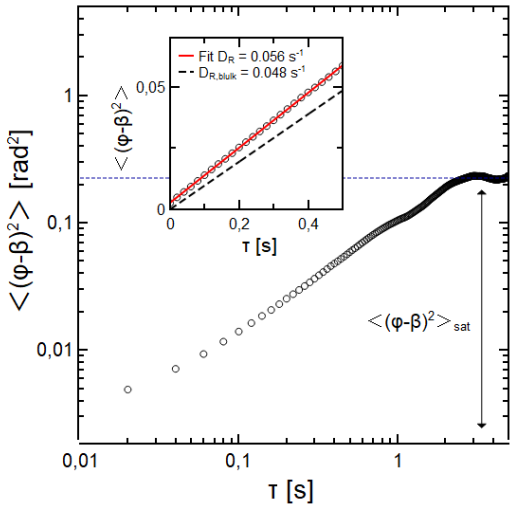

FIG. 6. Log-log graph of the mean squared angular displacement during the capture phase, before the full wrapping transition. Short times (inset) allows to fit the diffusion coefficient D_R while the plateau at large times evidences the angular confinement of the particle during this phase.

Appendix F: Comparison with pusher Pt-Si/H_2O_2 interaction with a GUV

The behavior of Cu-SiO_2 particles in glucose in the presence of giant unilamellar vesicles is very different from the one observed for the Pt-Si Janus colloids immersed in H_2O_2. This is shown in Figure 7 where the top row shows three snapshots taken at 1 s interval of a Pt-Si swimmer interacting with a GUV in H_2O_2. It clearly appears that the particle persistently orbits around the vesicle with $(\phi - \beta) \approx \pi/2$. The bottom row, instead, illustrates the case of a Cu-SiO_2 particle in glucose, which shows no persistent orbital motion and $(\phi - \beta) \approx 0$. The small variations of ϕ relatively to beta allow the particle to somewhat explore an arc of the GUV periphery. However, particle reorientation due to either hydrodynamic

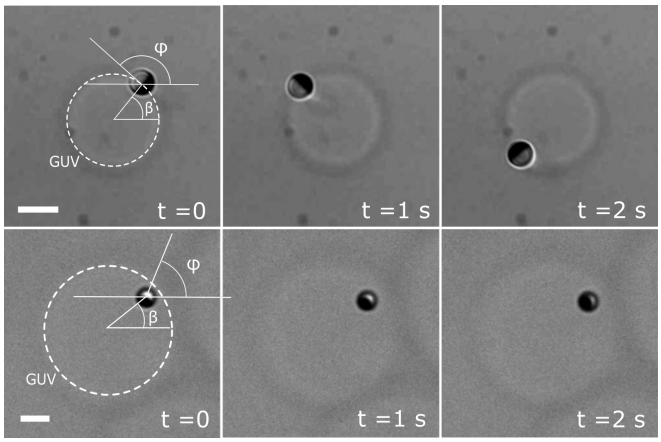

FIG. 7. (Top row) Snapshots of a Pt-Si Janus puller swimmer in H_2O_2 at the periphery of a GUV for three times spaced of 1 second. (Bottom row) Snapshots of a Cu@SiO_2 Janus in glucose during the capture phase at the periphery of a GUV at three different times.

attraction with the GUV or Brownian motion results into an averaged zero net motion on the vesicle periphery.

Appendix G: Stiffness and Diffusivity measurements

To estimate the diffusivity D_α and stiffness k that comes in the Kramers equation linking the hopping rate to the energy barrier E_b (see main text), we use the data of the variations of L during the capture phase. L is acquired by tracking the position of both the particle center-of-mass and the vesicle center-of-mass using Blender. The variations of L are translated in variations of the wrapping angle α ($\Delta L = R_P \Delta\alpha$). We can then compute the corresponding mean squared angular displacement of α and extract the diffusivity D_α from linear fits at short times since $\mathrm{MSAD}(\Delta t) = 2D_\alpha \Delta t$, as shown in Figure 8. The average for three trajectories yields $\langle D_\alpha \rangle = 0.021$ rad^{2}s^{-1}.

The variations of α are confined in an effective potential, which we can obtain experimentally under the assumption that the probability to find a particle at a given position is linked to the energy by the standard Boltzmann weight. Assuming a quadratic potential, we can extract a stiffness k by fitting the effective potential with a parabola. Average value $k = 38\ k_B T$ extracted from three parabolic fits is shown in Figure8 with the associated average parabola for the potential.

Appendix H: Movies

- S1 : MOVIE_S1_BRIGHTFIELD_60x
- S2 : MOVIE_S2_FLUORESCENCE_60x

[1] A. J. Goldmans, R. G. Cox, and H. Brenner, Slow viscous motion of a sphere parallel to a plane wall-1 motion through a quiescent fluid, Chemical Engineering Science **22**, 637651 (1967).
[2] P. G. Saffman and M. Delbrück, Brownian motion in biological membranes (diffusion), Biophysics **72**, 3111 (1975).
[3] F. Fessler, V. Sharma, P. Muller, and A. Stocco, Entry of microparticles into giant lipid vesicles by optical tweezers, Phys. Rev. E **107**, L052601 (2023).
[4] H. Turlier and T. Betz, Fluctuations in active membranes (2018), arXiv:1801.00176 [physics.bio-ph].
[5] W. Helfrich and R.-M. Servuss, Undulations, steric interaction and cohesion of fluid membranes, Il Nuovo Cimento D **3**, 137 (1984).

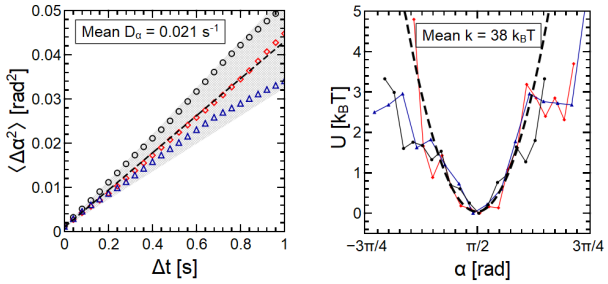

FIG. 8. (a) Mean squared angular displacement curve obtained from the variations of L for 3 trajectories with associated fits in plain lines. (b) Effective potential U obtained from position histogram. Black dashed line shows the mean quadratic potential extracted from fits of the 3 potentials, giving the a stiffness value k.